Ionic flexible capacitive three-dimensional force sensor for electromechanical signal monitoring

Zihan Lv 1, Lin Cheng 1*, Guanzheng Chen 1, Xuanzi Luo 1, Hang Yu 1, Hanxiao Zhang 1, Huaping Wu2* and Aiping Liu1*

***Abstract*—Accurate three-dimensional (3D) force sensing technology plays a crucial role in monitoring the electromechanical signals of the manipulator. Despite the design of various flexible capacitive 3D force sensors, their sensitivity often fails to meet the requirements for monitoring manipulators effectively. To address this issue, this work has designed an ionic flexible capacitive 3D force sensor with pyramidal microstructure. This sensor relies on the mechanical deformation of the pyramidal microstructure and the coupling of the capacitive effect of the electric double layer to output sensing information. Sensitivity of this sensor can reach 38.3 kPa^{-1}, and it has a fast response time (62 ms), excellent hysteresis and repeatability. With the application of back propagation neural network (BPNN), the accuracy of decoupling can be optimized, resulting in the error being reduced to 10^{-3}. The sensors have the ability to monitor electromechanical signals that can help the manipulator identify the topographic features of a target object, as well as monitor the gripping force of the manipulator and whether the target object is sliding. This unique 3D force sensor provides novel ideas for the design of new multi-dimensional force sensors, paving the way for the development of human-computer interaction and wearable devices.**

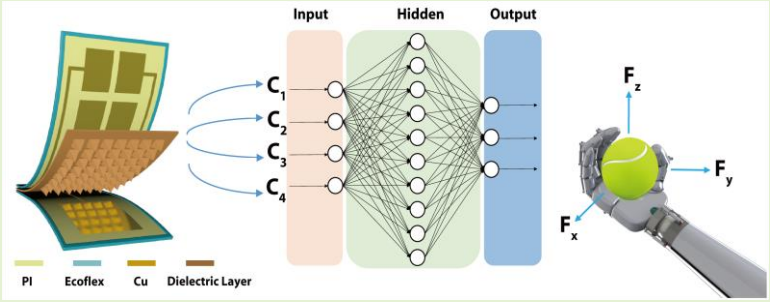

***Index Terms*—Flexible capacitive sensor; Three-dimensional force; Dielectric layer; Electromechanical signal.**

I. Introduction

With the continuous development of artificial intelligence technology [1], [2] and human-computer interaction [3], [4] as a tool capable of replacing human hands in grasping objects, the manipulator has become an indispensable machine in modern production and life. Theoretically, the manipulator should grasp the target object with a minimum critical force that can ensure stable grasp of the object without losing it. However, because of the limitations of technology, the manipulator can't ensure grasp an object by using minimum critical force always. So, people require a force sensitive sensor [5]-[7] as a medium to monitor the state of the manipulator during operation.

Manuscript received 28 Jane 2024; This work was supported by the National Natural Science Foundation of China (No. 12272351, 2372168, 11972323), the Youth Top-notch Talent Project of Zhejiang Ten Thousand Plan of China (No. ZJWR0308010), the Zhejiang Provincial Natural Science Foundation of China (No. Z24A020008 and LR20A020002), the "Pioneer" and "Leading Goose" R&D Program of Zhejiang (Grant no. 2023C01051).

Zihan Lv ,Lin Cheng , Guanzheng Chen , Xuanzi Luo , Hang Yu , Hanxiao Zhang and Aiping Liu are with the Center for Optoelectronics Materials and Devices, Key Laboratory of Optical Field Manipulation of Zhejiang Province, School of Science, Zhejiang Sci-Tech University, Hangzhou 310018, China (Corresponding authors e-mail: chenglin@zstu.edu.cn ; liuaiping1979@gmail.com).

Huaping Wu is with the Key Laboratory of Special Purpose Equipment and Advanced Processing Technology, Ministry of Education and Zhejiang Province, College of Mechanical Engineering, Zhejiang University of Technology, Hangzhou 310023, China (emails: wuhuaping@gmail.com).

At present, three-dimensional (3D) force sensors are the most commonly used medium for monitoring the working state of manipulators [8]-[10]. Compared to traditional rigid 3D force sensors [11], flexible 3D force sensors [12]-[15] possess good flexibility [16], high sensitivity [17] and large range [18], making them widely used in force information sensing in different scenarios. One key feature of 3D sensors is their ability to decompose force from space into forces in the three directions of X, Y, and Z axes. The force information in the X and Y axes represents tangential force, while the force information in the Z axis represents normal force. Generally speaking, based on the sensing mechanism, flexible 3D force sensors can be classified as piezoresistive [19]-[20], piezoelectric [21]-[23] or capacitive sensors [24], [25]. Among them, piezoresistive sensors have a simple structure, low cost, and suitable for testing in static environments. Their major drawbacks lie in their susceptibility to temperature disturbances which can cause drift. Piezoelectric sensors exhibit good dynamic response performance and fast response time. However, they cannot measure zero-frequency signals. Capacitive sensors exhibit high sensitivity, good repeatability, and the ability to respond to signals of various frequencies, making them a subject of extensive study [26]-[32]. The sensitivity of a capacitive 3D force sensor reflects the relationship between the relative capacitance change of the sensor outputs and the pressure applied to the sensor ($S=(\delta(\Delta C/C_0)/\delta P$). Higher sensitivity indicates that the sensor is more responsive to small pressure changes. While various flexible capacitive 3D force sensors have been designed to enhance sensitivity by innovating the dielectric layer material,

most sensors primarily rely on the deformation of the dielectric layer to alter the spacing and projection area of the top and bottom electrodes, or to change the dielectric constant of the dielectric layer [33]. Consequently, the sensitivity of sensors under this sensing mechanism may not meet the practical requirements for 3D force detection in manipulators.

Over the past decade, ionic sensing [34]-[37] had experienced rapid development. The mechanism of this sensing technology utilized the advantage of the supercapacitor characteristics of the electric double layer (EDL) that occur at the elastic electrolytic-electronic interface [38]-[40]. Flexible capacitive sensors based on ionic sensing mechanisms have high sensitivity [41]-[43], making them widely used in electronic skin [44], wearable electronic devices [45], biomedical [46] and other fields. Upon further exploration, it has been discovered that the presence of microstructures [47], [48] can greatly improve the sensitivity of ionic capacitive sensors [49]. This is attributed to the presence of air gap, compared to sensors without such air gap, sensors with pyramidal microstructures had greater change in the spacing between the top and bottom plates under the same pressure, it made a greater change in relative capacitance and the sensitivity also increases accordingly [50]-[52]. For instance, Bai et al. [53] proposed an ionic electron flexible pressure sensor with hierarchical structure based on PVA/H_3PO_4 composite, the sensitivity of the sensor can reach up to 3302.9 kPa^{-1}. Cho et al. [54] designed a high dielectric constant ionic gel based on a pyramidal structure and used it as a dielectric layer for a capacitive sensor, resulting in an improved sensitivity of the sensor to 41.6 kPa^{-1}. Presently, most capacitive sensors designed based on EDL effect detect forces in one dimension [55]. In practical applications, most of the forces exerted on the sensor come from 3D forces in space. Therefore, one-dimensional strain sensors cannot comprehensively convey the information of the spatial forces applied to the sensor.

Thus, this work presents an ionic flexible capacitive 3D force sensor based on the 1-Butyl-3-methylimidazolium bromide [BMIM/Br] ionic salt, PVDF-HFP (polyvinylidene fluoride-hexafluoropropylene copolymer) and HMDA (1,6-Hexanediamine) composite. Compared to conventional capacitive 3D force sensors, the sensor leverages the microstructure of the dielectric layer and the capacitance effect of EDL to improve the sensitivity of the sensor by increasing the specific capacitance, which can reach a maximum sensitivity of 38.3 kPa^{-1}. In addition, the dielectric layer containing ionic liquids contributes to the improvement of the sensor's response speed (63 ms for the loading process and 62 ms for the unloading process). Given the sensor's multiple coupling relationships, such as microstructure deformation and the double capacitance effect in the working state, a backpropagation neural network (BPNN) model is employed to map and calibrate the 3D force information, reducing prediction error to 10^{-3}. As a proof-of-concept, the flexible capacitive 3D sensor can assist the manipulator in assessing the topographical information of the target object, providing feedback, and allowing for the reasonable adjustment of the manipulator's gripping force (Fig. 1a). This highlights the potential applications of flexible capacitive 3D force sensors in mechanical manufacturing and human-computer interaction, facilitating remote control and monitoring of various parameters.

II. Experimental Section

A. Materials

1-Butyl-3-methylimidazolium bromide was purchased from Shanghai Aichun Biotechnology Co., Ltd. PVDF-HFP was purchased from Solvay S.A. Ecoflex was purchased from Smooth – On (0050, U.S.A). DMF (C_3H_7NO) (99.5%) was purchased from Aladdin Holdings Group Co., Ltd 1,6-Hexanediamine ($C_6H_{16}N_2$) (99.5%) was purchased from Aladdin Holdings Group Co., Ltd. Concave mold processed by PDMS and produced by Xiamen Qiepu Medical Technology Co., Ltd. The manipulator was an electric two-finger manipulator with model of 2F-85 purchased from Shanghai Huiteng Industrial Equipment Co., Ltd. All chemicals were used as received.

B. Preparation of dielectric layer materials

Dielectric layer was prepared from composite of ionic salt [BMIM/Br], hexamethylenediamine (HMDA) and PVDF-HFP. Initially, 0.7g of PVDF-HFP is dissolved in 9ml of DMF. The solution is then heated and stirred in a 60°C water bath for 4 hours. Subsequently, 0.3g of [BMIM/Br] is added, and the mixture is stirred until the ionic salt is completely dissolved. Following this, 0.01g of HMDA is added dropwise to the solution, which is then heated and stirred for approximately 8 hours. The resulting mixture is poured into a mold containing a pyramid structure, solidified at 60°C, and subsequently demolded to obtain the dielectric layer.

C. Preparation of flexible capacitive 3D sensor

The sensor consists of an electrode layer and a dielectric layer with an overall size of 12 × 12 mm. The electrode layer of the sensor consists of a copper tape (150 μm) and a PI film (50 μm), which were prepared as follows: Firstly, the predetermined model of the top electrode and bottom electrode was drawn on the computer. The top electrode measures 6×6 mm, while the bottom electrode consists of four 4×4 mm squares, with a distance of 6 mm between the centers of each pair. The laser was used to cut the copper tape, forming the patterned electrodes. After the copper tape was cut, the upper and lower electrode layers were transferred with PI film to complete the preparation of the electrodes. A dielectric layer was then added between the two electrode layers, and the top and bottom electrodes were connected using Ecoflex to encapsulate the sensor (Fig. 1b).

D. Characterization

The morphologies of the dielectric layer sample were investigated by a Field Emission Scanning Electron Microscope (FE-SEM, Hitachi S4800). The functional groups of the dielectric layer were determined by a Fourier transform infrared spectroscopy (FTIR, Nicolet iS50 Series) at 1650 cm-1. Capacitance characteristics and capacitance changes for the sensor during stressing were collected by a digital bridge (LCR) at the frequency of 100 kHz and a constant voltage of 1V via the conductive silver paste to contact the extension of electrode layers. Data of capacitance changes during 3D force calibration

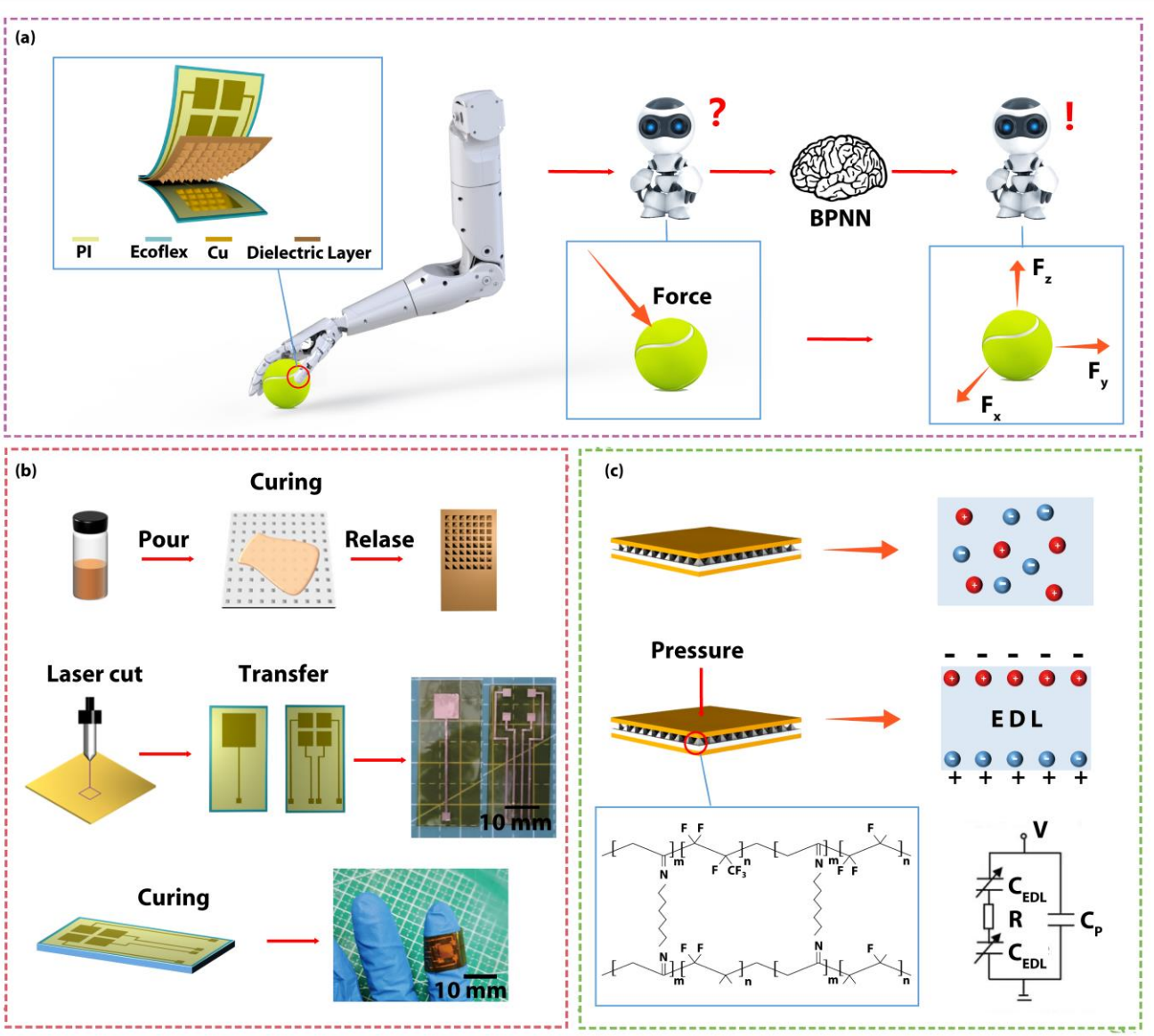

Fig. 1. (a) Schematic diagram of sensor using BPNN for 3D force detection. (b) Sensor's preparation process. (c) The principle of ion sensing and the equivalent circuit of the sensor.

and testing were collected using the data collector (DAQ-VANTECH USB_HRF4028).

III. RESULTS AND DISCUSSION

A. Fabrication and electrical characterisation of sensors

According to the preparation process in Fig. 1b, the flexible capacitive 3D force sensor shown in the structure of Fig. 1a can be obtained. The dielectric layer consisted of 10×10 micropyramidal structures, with the side length of a single micropyramid being 150 μm, the height of a single micropyramid being 300 μm, and the center distance between two micropyramids being 500 μm (Fig. S1). The high aspect ratio causes the micropyramid to have a larger longitudinal deformation when receiving pressure, which is beneficial to improving the sensitivity of the sensor. The dielectric layer is a composite material of ionic salt [BMMI/Br], HMDA and PVDF-HFP. HMDA is a cross-linking agent to promotecross-linking of PVDF-HFP and can effectively enhance the mechanical properties of PVDF-HFP (Fig. 1c). Cross-linking is accomplished by cleaving N-H in HDMA and forming C=N with C in PVDF-HFP (Fig. S2). In order to explore the effects of different concentrations of [BMIM/Br] and HMDA on the sensing properties and mechanical properties of the dielectric layer, a concentration gradient comparison experiment was designed. The dielectric layers with mass fractions of 20%, 30%, 40%, and 50% [BMIM/Br] were prepared by dissolving 1 g of PVDF-HFP in 10 mL of DMF solution, and the sensing performance was tested at a pressure of 0~0.5 kPa. As shown in Fig. S3a, it can be seen that at the same pressure, as the concentration of ionic liquids increased, the relative capacitance of the sensor changed also increased. However, at the stress-strain test of the dielectric layer, with the increasing concentration of [BMIM/Br], the mechanical properties of the dielectric layer continued to decrease. Comprehensive analysis, in the following experiment, the mass fraction of ionic salt was selected as 30%.

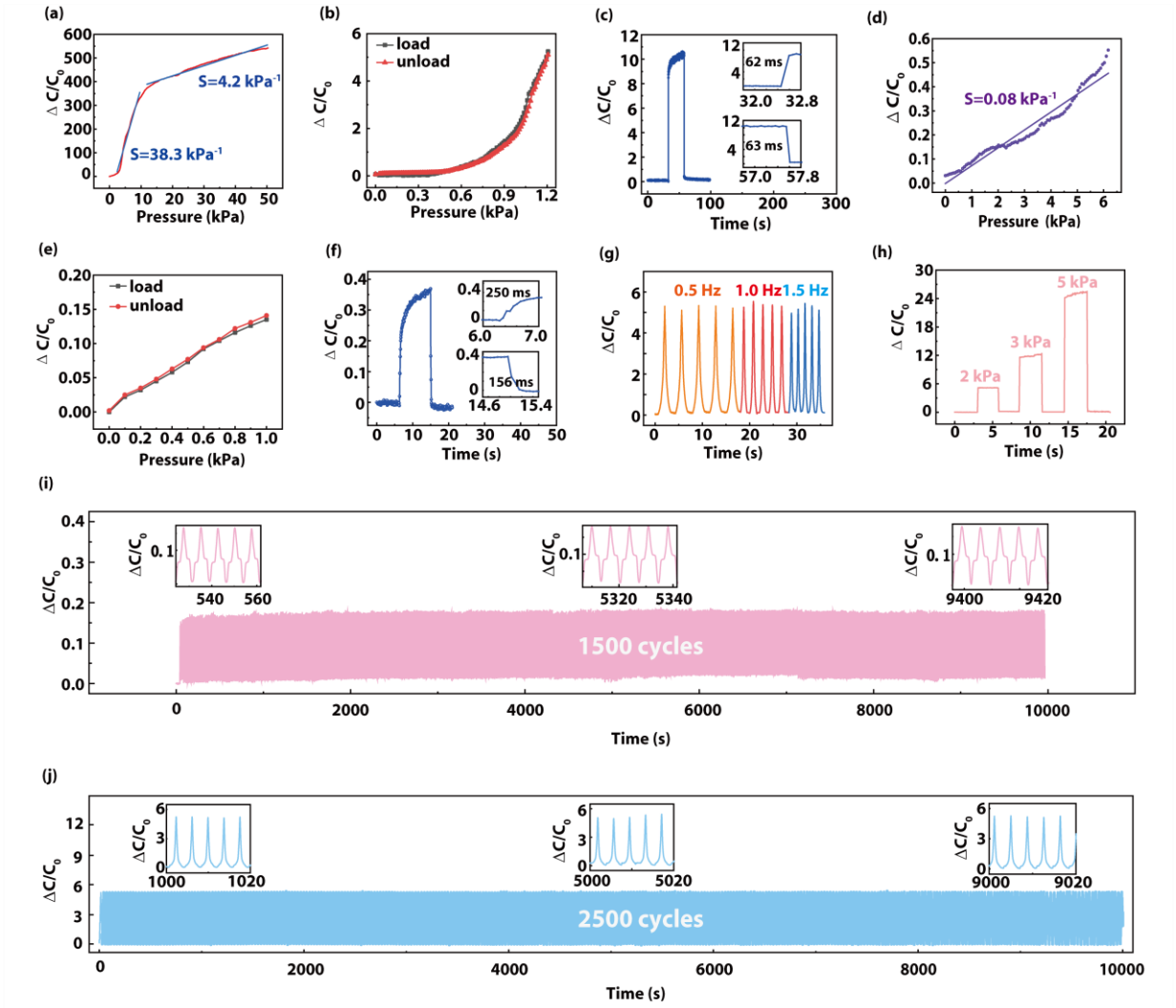

Fig. 2. Sensing performance of flexible capacitive 3D force sensor. (a) Sensor's normal sensitivity. (b) Sensor's normal hysteresis. (c) Sensor's normal response time. (d) Sensor's tangential sensitivity. (d) Sensor's tangential hysteresis. (f) Sensor's tangential response time. (g) Dynamic response of the sensor. (h) Static response of the sensor. (i) Sensor's tangential repeatability. (j) Sensor's normal repeatability.

Further, investigating the effect of dropwise addition of HMDA on sensing properties and mechanical properties of the dielectric layer under the addition of 30% [BMIM/Br] in Fig. S3b. The mass fractions of HMDA were respectively set to be 1%, 2%, 3%, 4%, and its sensing performance was tested under the pressure of 0~0.5 kPa in Fig. S3c. The results of tests show that relative capacitance change of the sensor decreased as the crosslinker concentration increased at the same pressure. However, the stress-strain test results show that the mechanical properties of the dielectric layer increase with the increasing concentration of HMDA. Therefore, the mass fraction of HMDA was selected as 1% in subsequent experiments in Fig. S3d. In order to verify the thin film prepared with this ratio of ion salts and crosslinkers has good mechanical properties, using the mechanical parameters of the material established a thin film model with thickness of 300 μm and dimensions with 8 mm×2 mm. The thin film generated maximum of 0.22 mm of strain with tensile force of 10 N by static finite element analysis.

The distinctive properties of this flexible capacitive 3D force sensor not only enable reliable and sustainable measurement of the applied 3D force but also facilitate sensitive pressure monitoring, as depicted in Fig. 2a. The relative capacitance change of the sensor depends on the mechanical deformation of the dielectric layer and the effect of EDL, positive and negative ions in the film move to both sides of the plate when the dielectric layer is mechanically deformed, the equivalent circuit is shown in Fig. 1c. The maximum sensitivity of 38.3 kPa^{-1} can be achieved within the pressure range of 0-10 kPa. This represents a substantial improvement compared to the sensitivities reported in Table S2. The finite element analysis of the dielectric layer and its microstructures is shown in Fig. S4. Additionally, controls were established using sensors prepared with dielectric layers lacking microstructures but containing [BMIM/Br], and dielectric layers lacking [BMIM/Br] but containing microstructures (Fig. S5). The results demonstrate a significant improvement in sensor sensitivity for detecting normal force when both microstructures and ionic liquids are present. For the tangential force test, as depicted in Fig. 2d,

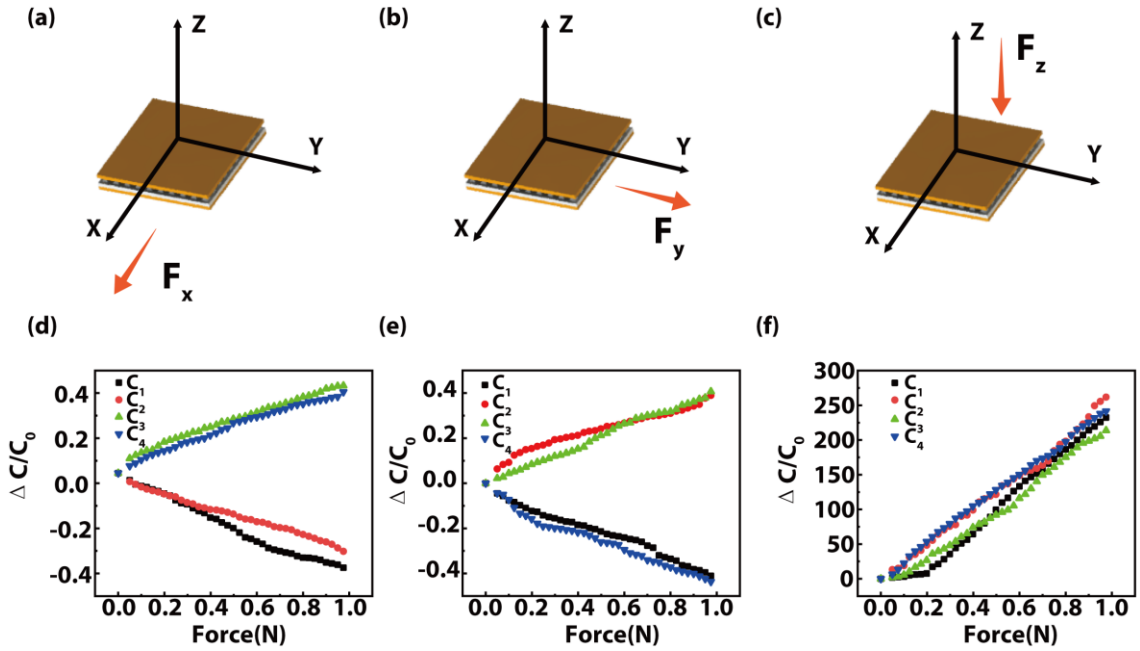

Fig. 3. Calibration of flexible capacitive 3D force sensor. (a) Schematic diagram of X-axis calibration. (b) Schematic diagram of Y-axis calibration. (c) Schematic diagram of Z-axis calibration. (d) Relationship between the force applied in X-axis and the relative capacitance variation. (e) Relationship between the force applied in Y-axis and the relative capacitance variation. (f) Relationship between the force applied in Z-axis and the relative capacitance variation.

a linear moving platform was employed to apply a tangential force (0-1 kPa) to the sensor. The sensor's tangential sensitivity measured at 0.08 kPa^{-1}. Furthermore, robustness and stability are also very important in practical applications. Fig. 2b and 2e demonstrate that when a loading-unloading cyclic force of 2 kPa is applied in the normal and tangential directions, respectively, the relative change curves of the transducer capacitance overlap almost exactly, with only a change of 0.5% observed. This exhibits favorable characteristics compared to the 3D force sensor without EDL, indicating excellent hysteresis characteristics of the sensor. The sensor exhibited a consistent sensing signal without signs of fatigue over 2500 repeated loading-unloading cycles (programmed through the mechanical test platform) under 2 kPa of normal pressure (Fig. 2j), attesting to its remarkable stability and long-term durability. Similarly, as shown in Fig. 2i, it exhibits satisfactory cyclic stability over 1500 cycles of tangential force (2 kPa). This is due to the fact that the change in tangential relative capacitance is due to the deformation of the Ecoflex, which has good mechanical properties, and thus 1500 cycles are sufficient to verify that the 3D force sensors have good tangential stability. The sensor exhibited rapid response times under normal and tangential pressures of 2 kPa, with loading and unloading times of 62 ms and 63 ms, respectively (Fig. 2c). In comparison, the response time of a sensor without the EDL effect is approximately 393 ms for loading and 562 ms for unloading (Fig. S6b), indicating that the EDL effect can enhance the sensor's response time. Tangential loading time of 250 ms and an unloading time of 156 ms (Fig. 2f). Additionally, when subjected to cyclic pressure at frequencies of 0.5 Hz, 1 Hz, and 1.5 Hz, the sensor demonstrated a stable dynamic response (Fig. 2g). It operated consistently at static pressures of 2 kPa, 3 kPa, and 5 kPa, with the relative capacitance change value at the sensor output remaining stable. This confirmed the sensor's dependable static response (Fig. 2h). The impact of the operating temperature on the sensor is also a critical parameter. Fig. S7a depicts the sensor placed in an environment where the external temperature linearly increased from 22°C to 80°C. The results indicate that the relative capacitance of the sensor output remains unaffected by the external temperature. Additionally, as depicted in Fig. S7b, when the sensor is subjected to a linear increase in external temperature (from 22°C to 80°C) and a pressure of 1.5 kPa (2.5 Hz), the relative capacitance of the sensor output remains stable.

To determine the optimal parameters for the height and width ratio of pyramidal microstructures, comparative experiments were conducted. Pyramidal microstructured media layers of two sizes were prepared: 300 μm × 200 μm (depicted in Figs. S8a and S8b) and 350 μm × 150 μm (depicted in Figs. S8c and S8d). These microstructures were tested for sensitivity, response time, and reproducibility across different aspect ratios (Figs. S9 -10). The pyramidal microstructure sensor with a size of 300 μm × 200 μm achieves a sensitivity of 36.2 kPa^{-1} (Fig. S9a) and loading and unloading response times of 100 ms and 105 ms, respectively (Fig. S9b), both lower than those of the 300 μm × 150 μm sensor. The pyramidal microstructure sensor with a size of 350 μm × 150 μm achieves a sensitivity of 42.8 kPa-1 (Fig. S10a) and response times of 63 ms for both loading and unloading (Fig. S10b). However, waveform distortion in the sensor output, indicated by the variation in relative capacitance during the repeatability test (Fig. S10c), suggests that molds of this size are prone to microstructure deformation during the demoulding process. Therefore, a size of 300 μm × 150 μm was determined as the optimal size.

B. Calibration of the flexible 3D force sensor

For the calibration of the flexible 3D force sensor, this work used a mechanical test platform and a linear moving platform to apply normal and tangential forces to the sensor, respectively.

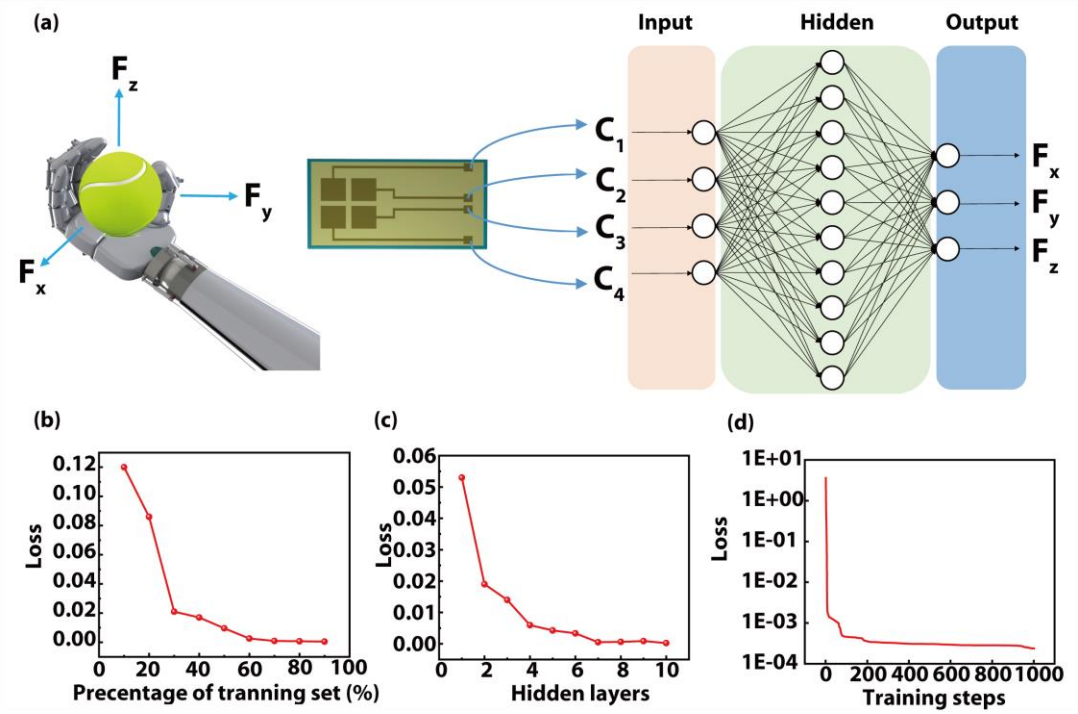

Fig. 4. Decoupling of flexible capacitive 3D force sensor. (a) The network structure of BPNN. (b) Effect of the number of training samples on decoupling accuracy. (c) Influence of the number of hidden layer nodes on the decoupling accuracy. (d) Training error curve of BPNN.

Simultaneously, a data collector was employed to capture the relative capacitance variations. The calibration curve of the sensor was established by systematically applying three-dimensional forces to the sensor. The calibration information sampling circuit can be seen in Fig. S11. The detection range for normal force was set at 0-1N (F_z), while for tangential force, it was 0-5N (F_x, F_y). As depicted in Fig. 3a and 3d, when a tangential force was applied along the X axis, the projection area of C_3 and C_4 on the top common plate and the bottom electrode layer increased, while the projection area with C_1 and C_2 decreased. Similarly, when a tangential force was applied along the Y axis, the projection area of C_2 and C3 on the top common plate and the bottom electrode layer increased, while the projection area with C_1 and C_4 decreased (Fig. 3b, 3e). When a normal force (F_z) was applied, the relative capacitance changes of C_1, C_2, C_3, and C_4 all exhibited a linear increase with the rise in normal force (Fig. 3c, 3f). Using the table (Table S1) to represent the relationship between each capacitor and the X-axis, Y-axis, and Z-axis components in 3D force testing when conducting 3D force measurements. When the capacitance change's rates of C_1 and C_2 are less than 0, while the capacitance change's rates of C_3 and C_4 are greater than 0, it indicates that the sensor is experiencing a force directed towards the positive X-axis, whereas a reverse situation signified a force directed towards the negative X-axis. Similarly, when the capacitance change's rates of C_1 and C_4 are less than 0, and the capacitance change's rates of C_2 and C_3 are greater than 0, it means the sensor is subjected to a force along the positive Y-axis, and conversely, towards the negative Y-axis. Additionally, when all capacitance change rates of C_1 to C_4 are less than 0, the sensor is experiencing a force towards the positive Z-axis, whereas a negative changed indicates a force directed towards the negative Z-axis. Due to the presence of the ionic liquid, the contact surface between the electrode and dielectric layer induced an electric double capacitance effect. Consequently, the relative capacitance of the sensor exhibited a more pronounced change under normal force compared to tangential force. The displacement of the plates and the dielectric layer is presented in Fig. S12.

C. Theoretical calibration of sensor and BPNN calibration

The decoupling of the 3D force involves breaking down the applied force into three axial components along the X, Y, and Z directions. Consequently, it is imperative to establish a mathematical correlation between the electrical output from the sensor and the mechanical input it receives. In our experimental setup, the crosslinking reaction between PVDF-HFP and HMDA significantly enhances the mechanical properties of the dielectric layer, imparting it with a degree of elasticity. This led us to propose that the alteration in the equivalent spacing between the two plates of the sensor occurs in a linearly superimposed manner. The theoretical calibration formula of the sensor represents the mapping relationship between the applied three-dimensional force and the relative capacitance output of the sensing element. This work charts the movement of the dielectric layer when the sensor is calibrating (Fig. S12), and subsequently employ a fourth-order polynomial fit to ascertain the connection between each axial force and the alteration in equivalent distance (Supporting Information Note1).

Despite the dielectric layer's elasticity, it still retains nonlinear factors such as microstructure and ionic liquids. This introduces nonlinearity and inhomogeneity in the input-output relationship of the sensor. Consequently, the decoupled results of the 3D force obtained from the theoretical formula may not fully capture the nuances of the 3D force information. To address this issue, this work had integrated a BPNN for the

purpose of decoupling 3D forces. The advantage of using BPNN lies in its capability to approximate complex function mapping relationships through the backpropagation algorithm. Additionally, the BPNN model is well-suited for handling large-scale datasets and can be trained and predicted in a relatively short time. Decoupling three-dimensional forces involves dealing with nonlinear relationships, making it suitable for employing approximation methods to construct function relationships. The network structure of BPNN is shown in Fig. 4a, which contains a hidden layer with a size of 10. Besides, the process of constructing the

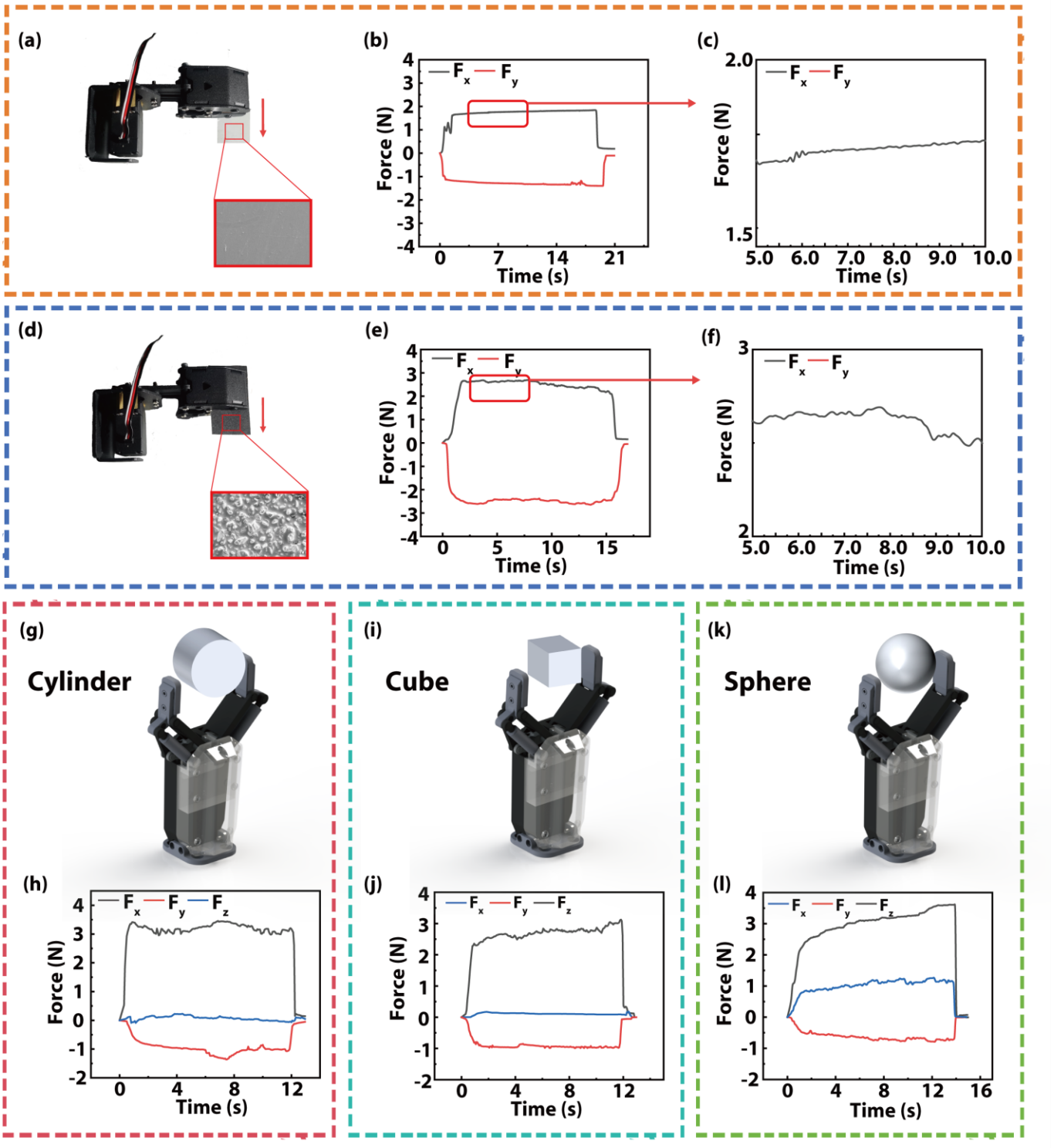

Fig. 5. Monitoring the topography information of the target object. (a) (b) (c) The optical image and relative capacitance changes curve of the sensor when grasping the PET film. (d) (e) (f) The relative capacitance changes curve of the sensor when grasping the sandpaper. (g) (j) The 3D force curve output by sensor when gripping the cylinder. (h) (k) The 3D force curve output by sensor when gripping the cube. (i) (l) The 3D force curve output by sensor when gripping the sphere.

decoupled model using BPNN proceeds as follows: Firstly, this study biases the calibration data by randomly selecting 70% of the data for the BPNN's training set and assigning the remaining 30% as the test sample. The study investigates the impact of the number of hidden layer nodes on decoupling accuracy, as depicted in Fig. 4c. Nevertheless, practical applications must consider factors such as computational complexity and processing speed. After further comprehensive evaluation, 10 nodes were chosen to be retained in this study. The study iteratively trained the BPNN to determine the minimum number of training samples required for accurate 3D force decoupling. The BPNN demonstrated effective mapping when the number of training samples accounted for approximately 70% or more of the total samples (Fig. 4b). Furthermore, as depicted in Fig. 4c, the training error steadily decreases with an increase in the number of iterations. Upon completion of 1000 iterations, the error decreases to 10^{-3}, as illustrated in Fig. 4d. Furthermore, a comparison between the response times of the sensor system utilizing theoretical decoupling (Supporting Information Note 1) and BPNN decoupling (Fig. S13) reveals that the computation time for BPNN decoupling (92 ms) closely matches that of theoretical decoupling (92.5 ms), indicating that the utilization of BPNN decoupling does not significantly impact the sensor's response speed.

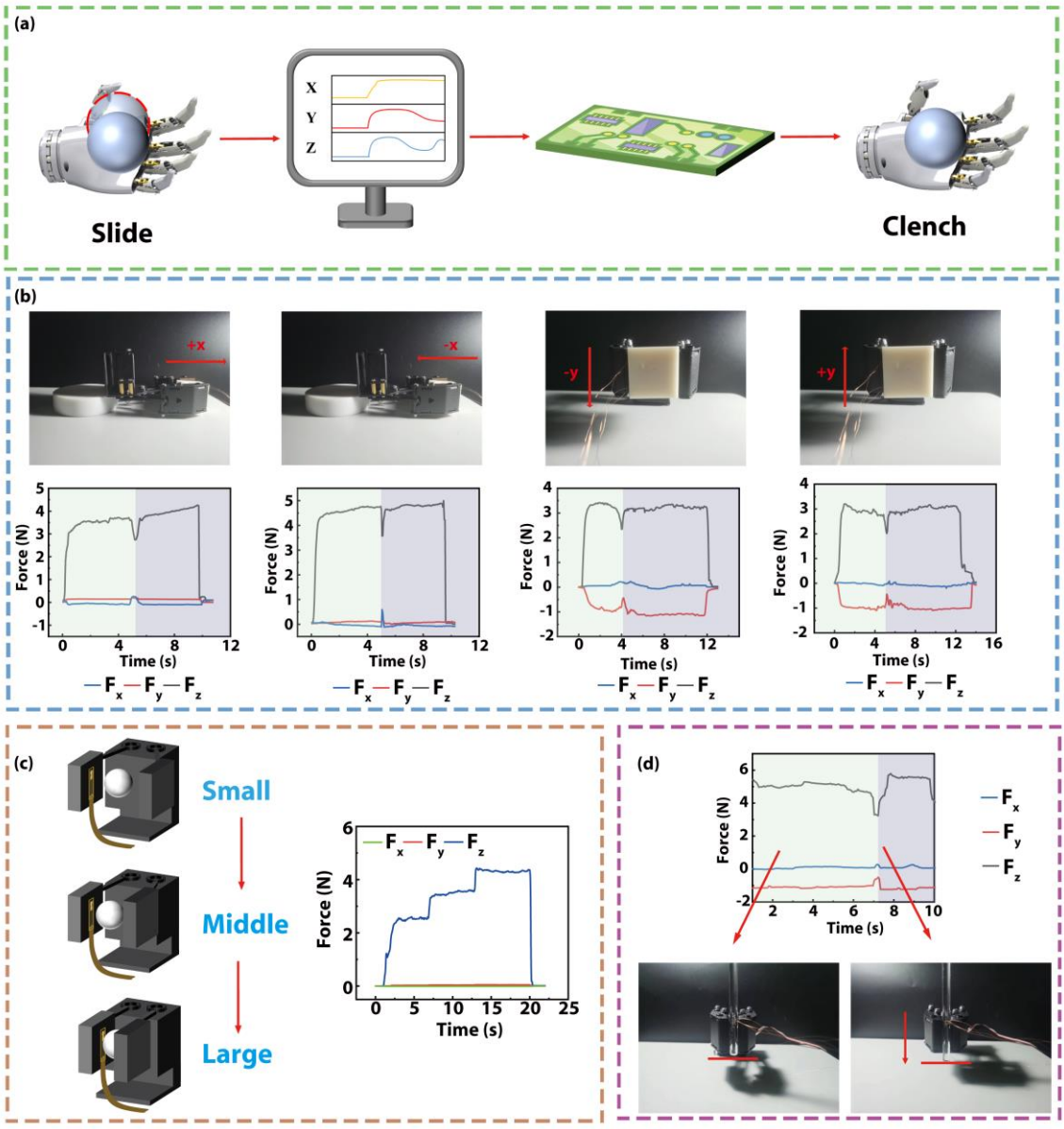

Fig. 6. Flexible capacitive 3D force sensor monitors the gripping strength and sliding status of the manipulator. (a) Control the gripping status of the manipulator. (b) The target object produces 3D force curve of the sensor output when sliding along the + X axis, -X axis, -Y axis, + Y axis, respectively. (c) Sensors monitor the gripping force of the manipulator. (d) Using glass rod simulated the control of the sliding b manipulator.

D. 3D force test and the error analysis

The specific steps of the 3D force test are as follows: Initially, ABS (acrylonitrile-butadiene-styrene copolymer) is selected as the 3D printing material, and slopes with inclinations of 30°, 45°, and 60° are fabricated using 3D printing technology.

Subsequently, each sensor is securely affixed to different slopes and connected to the test circuit. Finally, with the slope serving as the reference point, the electrical signals outputted by the sensor are recorded, and this process is repeated 10 times. The test outcomes reveal that when the sensor is subjected to spatial pressures at 30°, 45°, and 60° inclinations, the maximum relative capacitance changes for each sensing unit output are approximately 230, 190, and 160, respectively (Fig. S14). These results are then fed into theoretical formulas and BPNN models for decoupling. Using MATLAB, this work generated an error matrix depicting the components of the upward forces in the X, Y, and Z directions for varying angles (Fig. S15). Upon applying a 3D force at the same inclination, the error order for theoretical decoupling is approximately 10^{-1}, whereas for BPNN decoupling, the error order is around 10^{-3}. This indicates that after employing BPNN for decoupling the 3D force, the sensor exhibits high linearity and precise dimensional separation. As a result, the spatial 3D forces acting on the sensor can be more accurately discerned.

E. Application of flexible capacitive 3D force sensor

PET film and sandpaper were selected in the experiment to evaluate objects with different surface roughness. The SEM images of the PET film and sandpaper are presented in the inset of Fig. 5a and 5d. The PET film exhibited a smooth surface, whereas the sandpaper displayed a coarse texture. The procedure involved the manipulator gripping the material and moving it along the X axis at a speed of 150 mm/s. Subsequently, the value of the relative capacitance change outputted by each sensing unit of the sensor was recorded. After decoupling the results using BPNN, the experimental outcomes are depicted in the Fig. 5b and 5e. Notably, the tangential forces (F_x and F_y) outputted from the sensor exhibit smoother curves when gripping PET (Fig. 5c). Conversely, when the manipulator grasped the sandpaper, the shear curve output from the sensor displays distinct sawtooth peaks (Fig. 5f). This phenomenon indicates that the friction generated when the sensor moves on rough materials is greater than that on smooth materials. This provided strong evidence of the flexible capacitive 3D force sensor's excellent recognition capability. Further experiments involved manipulating objects of various shapes with a manipulator equipped with the flexible capacitive 3D force sensor (Fig. 5g-i). Simultaneously, the curves depicting the 3D force output of the sensor were captured (Fig. 5j-l). The results revealed that when the manipulator grasped different objects, the waveform of the corresponding 3D force curve varies. Consequently, the shape of the gripped object can be discerned based on the distinctive characteristics of the 3D force curve.

Through programmed control, the manipulator emulated the process of manually gripping plastic bottles and output the corresponding 3D force information, as illustrated in Fig. 6c. When the force exerted by the manipulator is approximately 2.5 N, there is no discernible changed in the plastic bottle. However, at around 3.5 N, the plastic bottle exhibits slight deformation. When the manipulator applied a force of roughly 4.5 N, the plastic bottle undergoes significant deformation and may even be subject to damage. This underscores the high sensitivity touch perception and real-time monitoring capabilities of the flexible capacitive 3D force sensor.

Given the ability to capture force information in real-time, the robot can effectively prevent issues such as overloading or damage to the target object. To validate the sensor's capacity to discern sliding behavior when the manipulator is grasping an object, the sensor is affixed to the manipulator for grasping a 3D printed cube. Subsequently, transient forces were applied to the object in both the +X, -X, +Y, and -Y directions, and the resulting 3D force curves from the sensor were recorded. As illustrated in Fig. 6b, when the manipulator securely griped the object, the output curved corresponding to the axial force undergoes a sudden change in signal regardless of the direction in which the target object is subjected to force. This is attributed to the static friction and pressure acting on the sensor in a steady state. When the object in question slides, both the static friction and pressure on the sensor change, consequently altering the signal of the force output by the sensor.

To address this, a feedback regulation closed-loop system was devised (Fig. 6a). This system aids the robot in adjusting the force when it grasps and slides a target object. The system's degree of adjustment allows the manipulator to securely grip the object with minimal critical force, preventing slippage. As depicted in Fig. 6d, a glass rod was affixed to the manipulator. When the glass rod slides, the sensor provided feedback in the form of three-dimensional force signals to the manipulator, which then increased its grasping force to counteract the sliding motion of the glass rod.

IV. CONCLUSION

In summary, a composite incorporating 1-butyl-3-methylimidazolium bromide ionic liquid [BMIM/Br] was employed as the dielectric layer to fabricate a flexible capacitive 3D force sensor. The integration of microstructure within the dielectric layer and the capacitive effect of the EDL were pivotal in augmenting the sensor's normal sensitivity, achieving a notable 38.3 kPa^{-1}. Moreover, the sensor demonstrated commendable hysteresis within a pressure range of 0-0.2 kPa, and maintained robust stability over 2500 cycles of normal forces and 1500 cycles of tangential force during load-unloading. To mitigate the influence of nonlinear factors on decoupling outcomes, BPNN was employed to refine the 3D force decoupling process of the sensor, reducing the error magnitude to 10^{-3}. This refinement satisfied the demands of high-precision 3D force decoupling in practical applications. As a demonstration of the application, the sensor not only identifies the shape and surface roughness of the target object, but also effectively monitors the robot's grasping status, including the force exerted during object manipulation and prevention of slipping. Thus, this work believes flexible capacitive 3D force sensor demonstrating potential applications in the domains of human-computer interaction and artificial intelligence in the foreseeable future.

REFERENCES

[1] S. Baek et al., "Flexible piezocapacitive sensors based on wrinkled microstructures: toward low-cost fabrication of pressure sensors over large areas," *RSC Adv.,* vol. 7, no. 63, pp. 39420-39426, 2017.

[2] Y. X. Xiong et al., "A flexible, ultra-highly sensitive and stable capacitive pressure sensor with convex microarrays for motion and health monitoring," *Nano Energy*, vol. 70, Apr, 2020.

[3] L. Cheng et al., "A highly sensitive piezoresistive sensor with interlocked graphene microarrays for meticulous monitoring of human motions," *J. Mater. Chem. C*, vol. 8, no. 33, pp. 11525-11531, Sep, 2020.

[4] L. Cheng et al., "A highly stretchable and sensitive strain sensor for lip-reading extraction and speech recognition," *J. Mater. Chem. C*, vol. 11, no. 25, pp. 8413-8422, Jun, 2023.

[5] J. H. Choi et al., "Graphene-based gas sensors with high sensitivity and minimal sensor-to-sensor variation," *ACS Appl. Nano Mater*., vol. 3, no. 3, pp. 2257-2265, Mar, 2020.

[6] Y. He, J. X. Wu, M. X. Lin et al., "Ionic flexible force sensors and their potential applications," *J. Mater. Chem. C*, vol. 9, no. 46, pp. 16378-16390, Dec, 2021.

[7] Y. Y. Zhu, S. W. Jiang, Y. Xiao et al., "A flexible three-dimensional force sensor based on PI piezoresistive film," *J. Mater*, vol. 29, no. 23, pp. 19830-19839, Dec, 2018.

[8] L. Q et al., "Graphene-paper pressure sensor for detecting Human motions," *ACS Nano*, vol. 11, no. 9, pp. 8790-8795, Sep, 2017.

[9] Y. Zhang et al., "Flexible and highly sensitive pressure sensor based on microdome-patterned PDMS forming with assistance of colloid self-assembly and replica technique for wearable electronics," *ACS Appl. Mater. Interfaces*, vol. 9, no. 41, pp. 35968-35976, Oct, 2017.

[10] S. M. Won et al., "Multimodal sensing with a three-dimensional Piezoresistive Structure," *ACS Nano*, vol. 13, no. 10, pp. 10972-10979, Oct, 2019.

[11] S. F. Zhao et al., "Three-dimensional distribution of sensitive field and stress field inversion of force sensitive materials under constant current excitation," *Sensors*, vol. 18, no. 3, Mar, 2018.

[12] Y. Song, F. L. Wang, and Z. Y. Zhang, "Decoupling research of a novel three-dimensional force flexible tactile sensor based on an improved BP algorithm," *Micromachines*, vol. 9, no. 5, May, 2018.

[13] R. Q. Li et al., "Research progress of flexible capacitive pressure sensor for sensitivity enhancement approaches," *Sens. Actuator A Phys*., vol. 321, Apr, 2021.

[14] H. Choi, and K. Kong, "A soft three-axis force sensor based on radially symmetric pneumatic chambers," *IEEE Sens. J*., vol. 19, no. 13, pp. 5229-5238, Jul, 2019.

[15] H. L. Meng et al., "A 3-D force sensor based on combination of magnetic and piezoresistive transduction," *IEEE Sens. J*., vol. 22, no. 4, pp. 3595-3604, Feb, 2022.

[16] J. Li et al., "Interfacially locked metal aerogel inside porous polymer composite for sensitive and durable flexible piezoresistive sensors," *Adv. Sci*, vol. 9, no. 23, Aug, 2022.

[17] L. Ding et al., "Three-dimensional structured dual-mode flexible sensors for highly sensitive tactile perception and noncontact sensing," *ACS Appl. Mater. Interfaces*, vol. 12, no. 18, pp. 20955-20964, May, 2020.

[18] B. Q. Nie et al., "Microfluidic tactile sensors for three-dimensional contact force measurements," *Lab Chip*, vol. 14, no. 22, pp. 4344-4353, 2014.

[19] J. Park et al., "Giant tunneling piezoresistance of composite elastomers with Interlocked microdome arrays for ultrasensitive and multimodal electronic skins," *Acs Nano*, vol. 8, no. 5, pp. 4689-4697, May, 2014.

[20] A. Huang et al., "A unique, flexible, and porous pressure sensor with enhanced sensitivity and durability by synergy of surface microstructure and supercritical fluid foaming," *Appl. Surf. Sci*., vol. 618, May, 2023.

[21] J. Park, M. Kim, Y. Lee et al., "Fingertip skin-inspired microstructured ferroelectric skins discriminate static/dynamic pressure and temperature stimuli," *Sci. Adv*., vol. 1, no. 9, Oct, 2015.

[22] X. Y. Song et al., "High performance and flexible piezoelectric composite incorporating zinc oxide grown on the oxidized nanocellulose by two-step hydrothermal process," *Appl. Surf. Sci*., vol. 649, Mar, 2024.

[23] R. B. Mishra, N. El-Atab, A. M. Hussain et al., "Recent progress on flexible capacitive pressure sensors: from design and materials to applications," *Adv. Mater. Technol*., vol. 6, no. 4, Apr, 2021.

[24] C. R. Yang, L. J. Wang, and S. F. Tseng, "Arrayed porous polydimethylsiloxane/barium titanate microstructures for high-sensitivity flexible capacitive pressure sensors," *Ceram. Int.*, vol. 48, no. 9, pp. 13144-13153, May, 2022.

[25] J. S. Meena et al., "Highly stretchable and robust textile-based capacitive mechanical sensor for human motion detection," *Appl. Surf. Sci.*, vol. 613, Mar, 2023.

[26] T. Y. Yao et al., "Highly sensitive capacitive flexible 3D-force tactile sensors for robotic grasping and manipulation," *J. Phys. D*., vol. 53, no. 44, Oct, 2020.

[27] B. Q. Nie et al., "Sensing arbitrary contact forces with a flexible porous dielectric elastomer," *Mater. Horizons*., vol. 8, no. 3, pp. 962-971, Mar, 2021.

[28] Y. C. Wang et al., "Mutual capacitive flexible tactile sensor for 3-D image control," *J Microelectromech Syst*., vol. 22, no. 3, pp. 804-814, Jun, 2013.

[29] E. Cagatay et al., "Flexible capacitive tactile sensors based on carbon nanotube thin films," *IEEE Sens. J*., vol. 15, no. 6, pp. 3225-3233, Jun, 2015.

[30] H. K. Lee et al., "Normal and shear force measurement using a flexible polymer tactile sensor with embedded multiple capacitors," *J Microelectromech Syst*., vol. 17, no. 4, pp. 934-942, Aug, 2008.

[31] Y. Huang et al., "A flexible three-axial capacitive tactile sensor with multilayered dielectric for artificial skin applications," *Microsyst. Technol*., vol. 23, no. 6, pp. 1847-1852, Jun, 2017.

[32] J. C. Yang et al., "Microstructured porous pyramid-based ultrahigh sensitive pressure sensor insensitive to strain and temperature," *ACS Appl. Mater. Interfaces*, vol. 11, no. 21, pp. 19472-19480, May, 2019.

[33] H. Z. Wang et al., "Flexible capacitive pressure sensors for wearable electronics," *J. Mater. Chem. C*, vol. 10, no. 5, pp. 1594-1605, Feb, 2022.

[34] X. L. Wang et al., "Microstructured flexible capacitive sensor with high sensitivity based on carbon fiber-filled conductive silicon rubber," *Sens. Actuator A Phys*., vol. 312, Sep, 2020.

[35] L. Mandal et al., "A auasi-liquid iontronic-electronic light-harvesting hybrid photodetector with giant response," *Adv. Mater*., vol. 24, no. 27, pp. 3686-3691, Jul, 2012.

[36] P. X. Han et al., "Lithium ion capacitors in organic electrolyte system: scientific problems, material development, and key technologies," *Adv. Energy Mater*., vol. 8, no. 26, Sep, 2018.

[37] S. H. Zhang et al., "Flexible highly sensitive pressure sensor based on ionic liquid gel film," Acs Omega, vol. 3, no. 3, pp. 3014-3021, Mar, 2018.

[38] Z. M. Lin et al., "Triboelectric nanogenerator enabled body sensor network for self-powered human heart-rate monitoring," *ACS Nano*, vol. 11, no. 9, pp. 8830-8837, Sep, 2017.

[39] L. Q. Ma et al., "A highly sensitive and flexible capacitive pressure sensor based on a micro- arrayed polydimethylsiloxane dielectric layer," *J. Mater. Chem. C*, vol. 6, no. 48, pp. 13232-13240, Dec, 2018.

[40] X. T. Shuai et al., "Highly sensitive flexible pressure sensor based on silver nanowires-embedded polydimethylsiloxane electrode with microarray structure," *ACS Appl. Mater. Interfaces*, vol. 9, no. 31, pp. 26314-26324, Aug, 2017.

[41] W. X. Han et al., "A self-powered wearable noninvasive electronic-skin for perspiration analysis based on piezo-biosensing unit matrix of enzyme/ZnO nanoarrays," *ACS Appl. Mater. Interfaces*, vol. 9, no. 35, pp. 29526-29537, Sep, 2017.

[42] J. H. Pu et al., "Human skin-inspired electronic sensor skin with electromagnetic interference shielding for the sensation and protection of wearable electronics," *ACS Appl. Mater. Interfaces*, vol. 10, no. 47, pp. 40880-40889, Nov, 2018.

[43] Y. P. Zang, F. J. Zhang, C. A. Di et al., "Advances of flexible pressure sensors toward artificial intelligence and health care applications," *Mater. Horizons*, vol. 2, no. 2, pp. 140-156, Mar, 2015.

[44] M. A. Lobo et al., "Wearables for pediatric rehabilitation: how to optimally design and use products to meet the needs of users," *Phys Ther*., vol. 99, no. 6, pp. 647-657, Jun, 2019.

[45] H. Jang et al., "Graphene-based flexible and stretchable electronics," *Adv. Mater*., vol. 28, no. 22, pp. 4184-4202, Jun, 2016.

[46] W. Li et al., "A porous and air gap elastomeric dielectric layer for wearable capacitive pressure sensor with high sensitivity and a wide detection range," *J. Mater. Chem. C*, vol. 8, no. 33, pp. 11468-11476, Sep, 2020.

[47] G. Z. Shen, "Recent advances of flexible sensors for biomedical applications," progress in natural science-materials international, vol. 31, no. 6, pp. 872-882, Dec, 2021.

[48] Y. Kim, H. Yang, and J. H. Oh, "Simple fabrication of highly sensitive capacitive pressure sensors using a porous dielectric layer with cone-shaped patterns," *Mater. Des*., vol. 197, Jan, 2021.

[49] S. Baek et al., "Flexible piezocapacitive sensors based on wrinkled microstructures: toward low-cost fabrication of pressure sensors over large areas," *RSC Adv*., vol. 7, no. 63, pp. 39420-39426, 2017.

[50] Y. S. Luo et al., "Flexible capacitive pressure sensor enhanced by tilted micropillar arrays," *ACS Appl. Mater. Interfaces*, vol. 11, no. 19, pp. 17796-17803, May, 2019.

[51] G. Zhu et al., "Self-powered, ultrasensitive, flexible tactile sensors based

on contact electrification," *Nano Lett*., vol. 14, no. 6, pp. 3208-3213, Jun, 2014.
[52] Y. Kumaresan, S. Ma, O. Ozioko and R. Dahiya, "Soft capacitive pressure sensor with enhanced sensitivity assisted by ZnO NW interlayers and airgap," *IEEE Sens. J.*, vol. 22, no. 5, pp. 3974-3982, March, 2022.
[53] N. N. Bai et al., "Graded intrafillable architecture-based iontronic pressure sensor with ultra-broad-range high sensitivity," *Nat. Commun*., vol. 11, no. 1, Jan, 2020.
[54] S. H. Cho et al., "Micropatterned pyramidal ionic gels for sensing broad-range pressures with high sensitivity," *ACS Appl. Mater. Interfaces*, vol. 9, no. 11, pp. 10128-10135, Mar, 2017.
[55] D. Kwon et al., "Highly sensitive, flexible, and wearable pressure sensor based on a giant piezocapacitive effect of three-dimensional microporous elastomeric dielectric layer," *ACS Appl. Mater. Interfaces*, vol. 8, no. 26, pp. 16922-16931, Jul, 2016.

Zihan Lv. received his master's degree from Zhejiang Sci-Tech University in 2022. His research interests are mainly in the development of flexible sensors based on multi-dimensional forces/strains to cope with complex external mechanical environments and flexible actuators to simulate external environments.

Lin Cheng. received her Ph.D. degree in Materials Science and Engineering from the Zhejiang Sci-Tech University in 2023 and a Bachelor's degree from Henan University in 2017. Since 2017 her has been working at the Department of Physics (Zhejiang Sci-Tech University), where her research mainly focuses on flexible sensors based on smart materials/structures and their applications in human-computer interaction.

Guanzheng Chen. received his B. S. degree from Zhejiang Sci-Tech University in 2022. He is currently studying in Zhejiang Sci-Tech University for his Master's degree. His research interests are developing novel materials for flexible sensors and their applications in wearable field.

Xuanzi Luo. received his B. S. degree in Guangdong Polytechnic Normal University in 2022. He is now studying for Master's degree in Zhejiang Sci-Tech University. His research interests involve solving multidimensional force perception problems in flexible tactile sensors with dual mode.

Hang Yu. received his B. S. degree in Civil Aviation University of China (CAUC) in 2022. He is now studying for Master's degree in Zhejiang Sci-Tech University. His research interests are mainly in the development of flexible sensors based on multi-dimensional forces/strains to cope with complex external mechanical environments.

Hanxiao Zhang. received his B. S. degree in Civil Aviation Flight School of China (CAFCS) in 2022. He is now studying for Master's degree in Zhejiang Sci-Tech University. His work focuses on the design of flexible sensor and applying it to the recognition for surface characteristics of touched objects with machine learning.

Prof. Huaping Wu received his Ph. D. degree in Engineering Mechanics from the Harbin Institute of Technology in 2009 and a Bachelor's degree from the Harbin Institute of Technology in 2002. He worked as a visiting scholar at the Kyoto University in 2014 and a postdoctoral research fellow at the City University of Hong Kong in 2012. He is currently a Professor in the School of Mechanical Engineering at Zhejiang University of Technology. His research mainly focuses on the mechanics of smart materials/structures, bionic machinery and bionic manufacturing, and flexible electronics devices.

Prof. Aiping Liu received her Ph. D. degree in Material Science from the Harbin Institute of Technology in 2008. She worked as a postdoctoral research fellow at the Nanyang Technological University from 2009 to 2011 and a visiting scholar at the University of Texas at Austin from 2019 to 2020. She is currently a Professor in the Department of Physics at Zhejiang Sci-Tech University. Her research mainly focuses on the functional inorganic/organic material, with special emphasis on developing novel materials including graphene with sensing and actuation characteristic for wearable physical/chemical sensors and intelligent actuators.